


Non-Hermiticity-induced topological transitions in long-range Su-Schrieffer-Heeger modelsChaohua Wu ^{1,2}, Ni Liu,^{4,*} Gang Chen,^{1,2,3,†} and Suotang Jia^{1,2}¹*State Key Laboratory of Quantum Optics and Quantum Optics Devices, Institute of Laser Spectroscopy, Shanxi University, Taiyuan 030006, China*²*Collaborative Innovation Center of Extreme Optics, Shanxi University, Taiyuan 030006, China*³*Collaborative Innovation Center of Light Manipulations and Applications, Shandong Normal University, Jinan 250358, China*⁴*Institute of Theoretical Physics, Shanxi University, Taiyuan 030006, China*

(Received 18 May 2022; accepted 7 July 2022; published 19 July 2022)

The interplay of topology and non-Hermiticity opens a new avenue for engineering novel topological matter and generating various unique effects. Here, we demonstrate that the non-Hermiticity can induce rich topological phase transitions in a long-range Su-Schrieffer-Heeger model. We find that the non-Hermiticity is able to drive topological transitions between different winding numbers: $\nu = 0 \rightarrow 1$ and $2 \rightarrow 1$. These topological phase transitions can be characterized by the bulk band gap, edge states, complex Zak phase, and hidden Chern number. Interestingly, by extending to more general long-range Su-Schrieffer-Heeger lattices, the non-Hermiticity can drive exotic transitions associated with the corresponding Hermitian topological phases. Finally, we demonstrate the experimental feasibility of our scheme in an electric circuit system. Our paper could be useful for the study of non-Hermitian topological states and their device applications.

DOI: [10.1103/PhysRevA.106.012211](https://doi.org/10.1103/PhysRevA.106.012211)**I. INTRODUCTION**

As a complex extension of conventional Hermitian systems, non-Hermitian systems have garnered great interest both theoretically and experimentally in recent years [1–5]. Besides being ubiquitous in nature, the non-Hermitian systems exhibit some hallmark features such as nonorthogonal eigenvectors [6,7], exceptional points [8,9], and unconventional localization [10,11]. Remarkably, there have been considerable efforts in exploring the interplay of non-Hermiticity and topological physics [12,13]. The topological open systems described by non-Hermitian Hamiltonians exhibit a rich variety of unique properties with no counterpart in the traditional Hermitian case, including novel topological invariants [14–17], non-Hermitian skin effect [18–25], non-Bloch bulk-edge correspondence [26–33], Weyl exceptional rings [34,35], and novel topological classifications with new symmetries [36–39]. Moreover, the unconventional and intriguing phenomena of non-Hermitian topological systems have profound applications in topological lasing [40,41], enhanced sensing [42–44], and topological light funneling and steering [45,46].

Recently, due to the flexible tunability and fine controllability of gain and loss in photonic lattices, electrical circuits, and ultracold atoms, non-Hermitian topological phases with complex on-site potential have been considered. A paradigmatic example is the non-Hermitian Su-Schrieffer-Heeger (SSH) model with \mathcal{PT} symmetry, where the non-Hermiticity

has no effect on the topological phases [47–50]. Intriguingly, a transition from trivial to topological nontrivial phases can emerge solely by controlling gain and loss possessing specific symmetry. Such topological phase transitions (TPTs) driven by non-Hermiticity have been explored in one-dimensional topological insulators [51–55], Chern insulators [56,57], higher-order topological insulators [58,59], and quantum spin Hall insulators [60], where the topological phases are divided into trivial and nontrivial ones. A natural question is what topological phase transitions can be induced by the non-Hermiticity in topological systems with rich topological phases (e.g., high winding number).

In this paper, we address this question by considering a non-Hermitian long-range SSH lattice, in which the complex on-site potentials and the third nearest-neighbor hopping are included. We find that the non-Hermiticity can drive topological transitions between different winding numbers: $\nu = 0 \rightarrow 1$ and $2 \rightarrow 1$. The topological phase transitions are characterized by the closing and reopening of the band gap, topological edge states, complex Zak phase, and hidden Chern number. By extending to the more general long-range SSH model, it is found that the non-Hermiticity drives exotic topological transitions associated with the topological phases of the corresponding Hermitian case. Finally, a simple experimental scheme based on electric circuits is proposed. Our paper could be useful for exploring non-Hermitian topological states and their device applications.

II. MODEL AND HAMILTONIAN

As shown in Fig. 1(a), we consider a one-dimensional extended SSH model with staggered nearest-neighbor

*Corresponding author: liuni2011520@sxu.edu.cn

†Corresponding author: chengang971@163.com

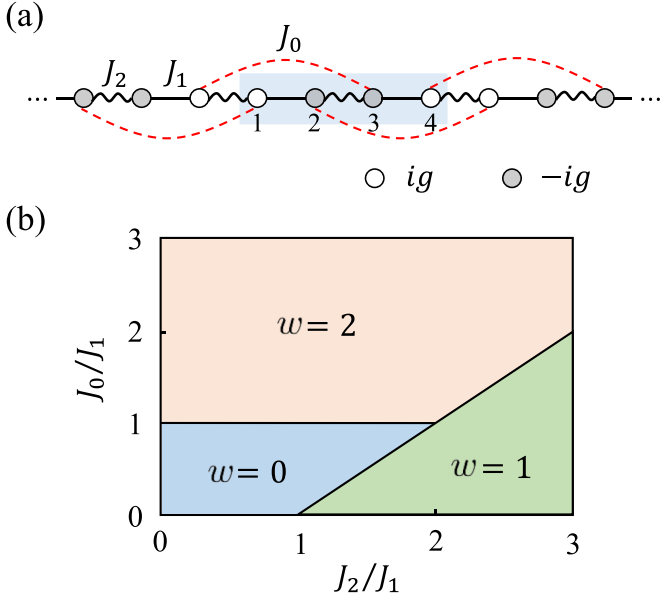


FIG. 1. (a) Schematic of the non-Hermitian SSH model with staggered nearest-neighbor hoppings J_1 (straight lines) and J_2 (wavy lines), and long-range hopping J_0 (red dashed lines). The open circles (filled circles) indicate positive (negative) imaginary parts, $\pm ig$. Each unit cell (shaded region) contains four sites labeled by $\{1, 2, 3, 4\}$. (b) Phase diagram of the Hermitian long-range SSH model with $g = 0$, i.e., the Hamiltonian (2), where $J_1 = 1$ is set as the energy unit. The winding number of each phase has $w = \{0, 1, 2\}$.

hoppings J_1 and J_2 , and long-range hopping J_0 that preserves chiral symmetry. Each unit cell contains four sites (labeled by $\{1, 2, 3, 4\}$) with the complex on-site potentials $(ig, -ig, -ig, ig)$. The corresponding Hamiltonian is written as

$$H = H_S + H_N \quad (1)$$

with

$$H_S = \sum_j^L [J_1(a_{j,1}^\dagger a_{j,2} + a_{j,3}^\dagger a_{j,4}) + J_2(a_{j,2}^\dagger a_{j,3} + a_{j,4}^\dagger a_{j+1,1}) + J_0(a_{j,1}^\dagger a_{j-1,2} + a_{j,3}^\dagger a_{j-1,4}) + \text{H.c.}] \quad (2)$$

and

$$H_N = ig \sum_j^L (a_{j,1}^\dagger a_{j,1} - a_{j,2}^\dagger a_{j,2} - a_{j,3}^\dagger a_{j,3} + a_{j,4}^\dagger a_{j,4}), \quad (3)$$

where $a_{j,l}^\dagger$ ($l = 1, 2, 3, 4$) and $a_{j,l}$ are the creation and annihilation operators at site l in the unit cell j , and $L = 4N$ is the length of the lattice with N being the number of the unit cells. H_S and H_N describe the Hamiltonians of the long-range SSH model and the non-Hermitian term, respectively.

In the momentum space, the Hamiltonian (1) is rewritten as

$$H(k) = \begin{pmatrix} ig & h_k & 0 & J_2 e^{-ik} \\ h_k^* & -ig & J_2 & 0 \\ 0 & J_2 & -ig & h_k \\ J_2 e^{ik} & 0 & h_k^* & ig \end{pmatrix}, \quad (4)$$

with $h_k = J_1 + J_0 e^{-ik}$. Note that $H(k)$ satisfies a pseudo-anti-Hermiticity, $\eta H^\dagger(k) \eta^{-1} = -H(k)$ with $\eta = \sigma_0 \otimes \sigma_z$. This symmetry induces a nontrivial topology with pairwise eigenvalues $E(k) = -E^*(k)$. In addition, it also possesses particle-hole symmetry with $\eta H^*(k) \eta^{-1} = -H(-k)$, time-reversal symmetry $\mathcal{T}_+ H \mathcal{T}_+^{-1} = H(-k)$ with $\mathcal{T}_+ = \sigma_0 \otimes \sigma_0$, and anti- \mathcal{PT} symmetry $(\mathcal{PT}) H(k) (\mathcal{PT})^{-1} = -H(k)$ with $\mathcal{P} = i\sigma_x \otimes \sigma_y$ and \mathcal{T} being the complex conjugation operator. Here, $\sigma_{x,y,z}$ are the Pauli matrices and σ_0 is the 2×2 identity matrix. Therefore, the system belongs to the BDI class in the non-Hermitian Altland-Zirnbauer topological classification [36]. The corresponding topological invariant is governed by the winding number ν .

In the Hermitian case (i.e., $g = 0$), the Hamiltonian (2) reduces to the long-range SSH model with $H_S(k) = h_x(k)\sigma_x + h_y(k)\sigma_y$, where $h_x(k) = J_1 + J_2 \cos k + J_0 \cos(2k)$ and $h_y(k) = J_2 \sin k + J_0 \sin(2k)$. The topological properties can be characterized by the winding number $w = \frac{1}{2\pi} \int_{-\pi}^{\pi} dk \frac{h_x \partial_k h_y - h_y \partial_k h_x}{h_x^2 + h_y^2}$ [49]. Figure 1(b) shows the topological phase diagram as functions of J_2/J_1 and J_0/J_1 . It can be found that three topological phases can be clearly identified with $w = 0, 1$, and 2 . Compared with the standard SSH model which has two phases with $w = 0$ and 1 , the long-range hopping provides richer topological phases with higher winding number. According to the bulk-boundary correspondence, the number of pairs of edge states corresponds to w , and the pairs are protected by the chiral symmetry.

In previous studies of non-Hermitian driven topological transition, the emergence of non-Hermitian topological phases as well as the corresponding Hermitian topological phases are divided into trivial and nontrivial ones. In a one-dimensional system, it was shown that the winding number transitions from $\nu = 0$ to 1 as the non-Hermitian parameter increases. Yet, the effects of non-Hermiticity in topological systems with rich topological phases (e.g., $w = 0, 1, 2$) have not been explored. In the following, we focus on the interplay of the non-Hermiticity with anti- \mathcal{PT} symmetry and the long-range SSH model admitting multiple topological phases, and show that the non-Hermiticity can induce rich topological phase transitions.

Note that the non-Hermitian long-range SSH model considered here does not exhibit the non-Hermitian skin effect. Thus, the topological properties can be characterized by the non-Hermitian extension of the Zak phase in the Brillouin zone [48]. Hereafter, we set $J_1 = 1$ as the energy unit for simplicity.

III. NON-HERMITICITY-INDUCED TOPOLOGICAL TRANSITIONS

Before discussing the topological phase transition, we consider the eigenvalues of the Hamiltonian (4), which is given as

$$E_{\pm, \pm}(k) = \pm \sqrt{A - g^2 \pm 2J_2 \sqrt{B - g^2}}, \quad (5)$$

where $A = J_1^2 + J_2^2 + J_0^2 + 2J_0 J_1 \cos k$ and $B = J_1^2 \cos^2(k/2) + J_0^2 \cos^2(k/2) + 2J_0 J_1 \cos(k/2)$. The bands $E_{+,+}$ ($E_{-,-}$) and $E_{+,-}$ ($E_{-,-}$) touch at $k = \pm\pi$ when $g = 0$. Particularly, the energy gap between the bands $E_{+,-}$ and $E_{-,+}$ at $k = 0$ is

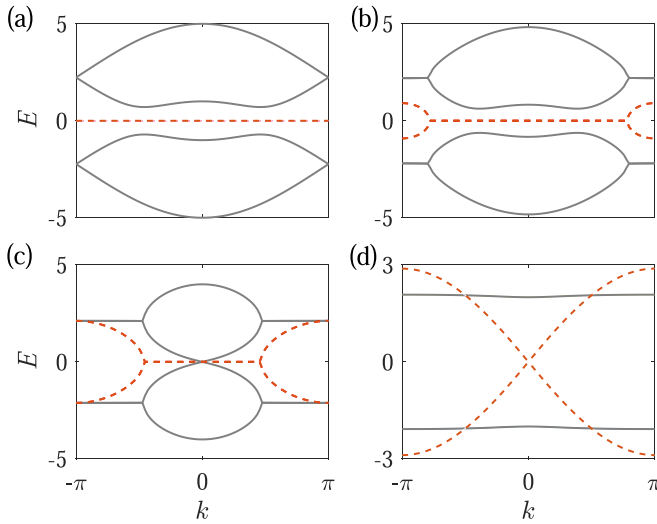


FIG. 2. Band structures of the Hamiltonian (4) for $g = 0$ (a), $g = 1$ (b), $g = \sqrt{5}$ (c), and $g = 3$ (d), when $J_0 = 2$ and $J_2 = 2$. The gray and red dashed curves indicate the real and imaginary parts of the energy spectrum, respectively. We have taken $J_1 = 1$ as the unit of energies.

obtained as

$$\Delta E = 2J_2 - 2\sqrt{(J_0 + J_1)^2 - g^2}, \quad (6)$$

which is a function of the non-Hermitian parameter g . It follows that ΔE vanishes when $g = \sqrt{(J_0 + J_1)^2 - J_2^2}$. Moreover, all eigenvalues become complex with nonzero imaginary part when $g > J_0 + J_1$. This non-Hermitian tuned band gap implies the existence of topological phase transition.

A. Topological transition with $\nu = 2 \rightarrow 1$

We start by considering the contribution of the non-Hermiticity in the high-winding number phase by choosing $J_0 = 2$ and $J_2 = 2$, which is located in the $w = 2$ topological phase without gain and loss, as shown in Fig. 1(b). Figure 2 shows the band structures for different g . It is clear that the edge degenerate points at $k = \pi$ with $g = 0$ [Fig. 2(a)] turn into exceptional points in the presence of the non-Hermitian parameter g [Fig. 2(b)], which is associated with the anti- \mathcal{PT} symmetry. With the increasing of g , the exceptional points gradually move toward the center of the Brillouin zone. At the critical value $g = \sqrt{5}$ [Fig. 2(c)], the middle two bands ($E_{+,-}$ and $E_{-,+}$) touch around $\text{Re}(E) = 0$ at $k = 0$, and reopen for $g > \sqrt{5}$. This implies a topological transition occurs at this critical point. Further increasing g , the pairs of upper and lower bands overlap and have the split imaginary bands when $g > 3$ [Fig. 2(d)]. These critical points are consistent with the analytical results.

For a deeper insight into the topological phase transition, we plot the energy spectrum as a function of g , as shown in Figs. 3(a) and 3(b). It can be seen that as g increases, the bulk gap closes and reopens at the critical point $g \approx \sqrt{5}$ [black dashed line in Fig. 3(a)], indicating the emergence of a topological phase transition. Notably, the midgap states always exist. To further illustrate this point, we plot the

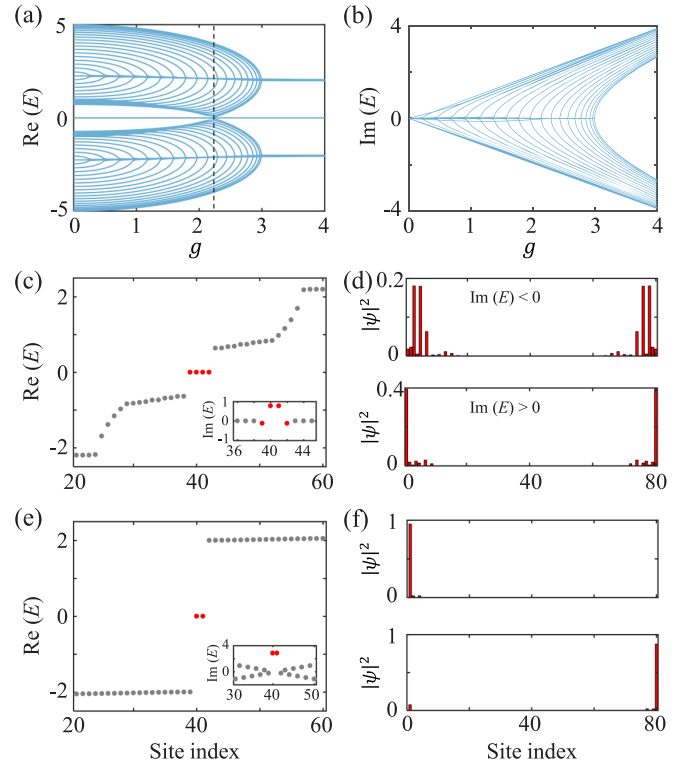


FIG. 3. The real (a) and imaginary (b) energy spectra of the Hamiltonian (1) as functions of g , when $J_0 = 2$ and $J_2 = 2$. (c) The real energy spectra with $g = 1$. The inset shows the corresponding imaginary eigenvalue. The red dots denote the eigenstates with $\text{Re}(E) = 0$. (d) The probability distributions of the zero-energy edge states corresponding to (c). (e) and (f) show the same as (c) and (d) but $g = 3$. Here, we choose $N = 20$.

energy spectrum for $g = 1$ in Fig. 3(c). There are four states with $\text{Re}(E) = 0$ in the gap. A pair of degenerate states satisfies $\text{Im}(E) > 0$ and another one satisfies $\text{Im}(E) < 0$. The corresponding probability distributions of these two pairs of states are shown in Fig. 3(d), which are localized at the boundary of the lattice. A remarkable difference is that the edge states with $\text{Im}(E) > 0$ are strongly localized at the two end sites while the edge states with $\text{Im}(E) < 0$ are not. Figures 3(e) and 3(f) show the energy spectrum and the midgap edge states distribution for $g = 3$, respectively. In this case, there are only two degenerate states in the gap. Each state with $\text{Re}(E) = 0$ is localized at the left or right end of the lattice. These indicate that the non-Hermitian parameter g indeed leads to a topological phase transition from $\nu = 2$ to 1, according to the bulk-boundary correspondence. Note that the non-Hermitian winding number ν is further illustrated in Sec. III C.

B. Topological transition with $\nu = 0 \rightarrow 1$

We further assess how the non-Hermiticity affects the topological properties in the trivial phase with $w = 0$. For simplicity, we choose $J_0 = 0.2$ and $J_2 = 0.5$ as an example. From Eq. (6), the bulk gap between the bands $E_{+,-}$ and $E_{-,+}$ closes at $k = 0$, when $g = \sqrt{1.19}$. With a larger $g > 1.2$, all eigenvalues become complex with nonzero imaginary part.

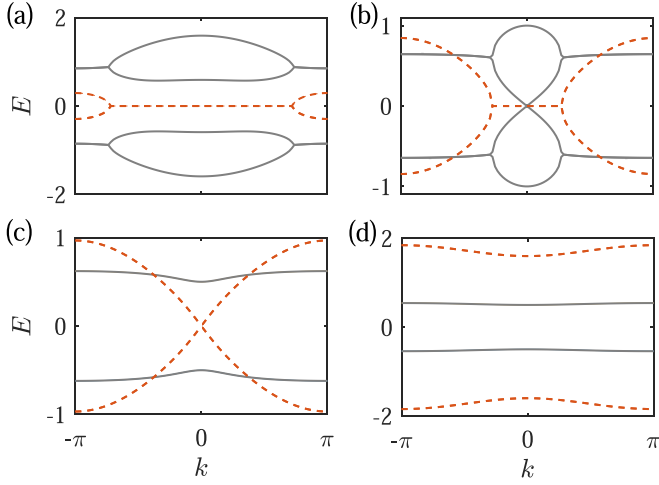


FIG. 4. Band structures of the Hamiltonian (4) for $g = 0.5$ (a), $g = \sqrt{1.19}$ (b), $g = 1.2$ (c), and $g = 2$ (d), when $J_0 = 0.2$ and $J_2 = 0.5$. The gray and red dashed curves indicate the real and imaginary parts of the energy spectrum, respectively.

These results are further clarified in Fig. 4, which indicates the existence of a topological phase transition at the critical point $g = \sqrt{1.19}$.

In Figs. 5(a) and 5(b), we plot the real and imaginary parts of the energy spectrum as functions of g . As we can see from the real energy spectrum, the bulk states close and reopen at $g \approx 1.09$ (black dashed line), which is consistent with Fig. 4(b). The states with $\text{Re}(E) = 0$ exist in the gap for $g > 1.09$. In Figs. 5(c) and 5(d), we plot the energy spectra and the density distributions of the midgap states with $g = 1.5$. Two degenerate states occur in the gap and are strongly localized at the end of the lattice. Obviously,

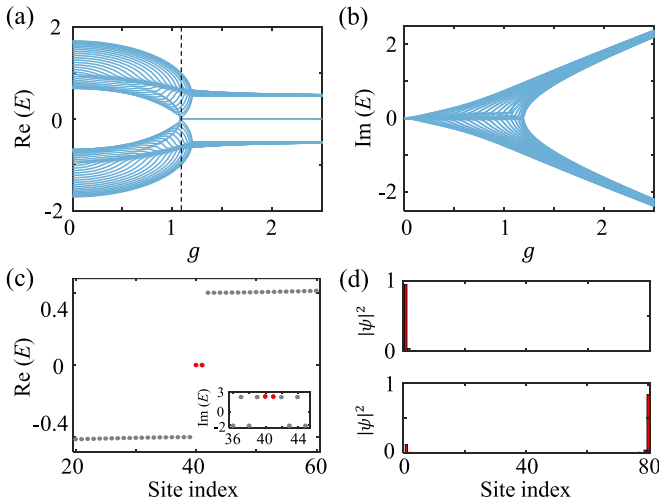


FIG. 5. The real (a) and imaginary (b) energy spectra of the Hamiltonian (1) as functions of g , when $J_0 = 0.2$ and $J_2 = 0.5$. (c) The real energy spectrum with $g = 1.5$. The inset shows the corresponding imaginary eigenvalue. Red dots denote the eigenstates with $\text{Re}(E) = 0$. (d) The probability distributions of the zero-energy edge states corresponding to (c). Here, we choose $N = 20$.

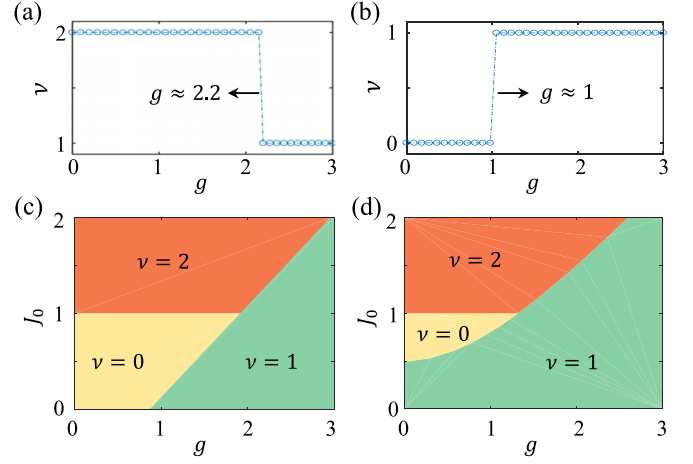


FIG. 6. (a, b) The winding numbers ν as functions of g for $\{J_0 = 2, J_2 = 2\}$ (a) and $\{J_0 = 0.2, J_2 = 0.5\}$ (b). (c, d) Phase diagrams of ν in the J_0 - g plane for $J_2 = 0.5$ and $J_2 = 1.5$, respectively.

the non-Hermiticity drives a topological transition from the trivial to nontrivial ($\nu = 1$) topological phases, which can be characterized by the closure of the band gap in the momentum space.

C. Characterization of the topological transition

As demonstrated above, the closings and reopenings of the bulk band gaps and the emergence of the gapless edge states indicate the change of the bulk topological properties. Here, we clarify topological invariants to characterize the topological phase transition.

The non-Hermitian Zak phase of the n th band is defined as $\mathcal{Z}_n = i \oint dk \langle \varphi_n | \partial_k | \psi_n \rangle$, where $|\psi_n\rangle$ and $|\varphi_n\rangle$ are the right and left Bloch eigenstates satisfying $H|\psi_n\rangle = E_n|\psi_n\rangle$, $H^\dagger|\varphi_n\rangle = E_n^*|\varphi_n\rangle$, and $\langle \varphi_n | \psi_m \rangle = \delta_{mn}$. For our system, the topological number can be described by the partial global Zak phase summed over for all occupied bands below the gap [51,61]:

$$\mathcal{Z} = \mathcal{Z}_1 + \mathcal{Z}_2. \quad (7)$$

Here, $E_{1,2,3,4}$ corresponds to the energy bands $\{E_{-,-}, E_{-,+}, E_{+,-}, E_{+,+}\}$, respectively, with the corresponding wave functions $|\psi_{1,2,3,4}\rangle$. The non-Hermitian winding number is obtained as $\nu = \mathcal{Z}/2\pi$.

In Figs. 6(a) and 6(b), we calculate the winding numbers ν as functions of g with $\{J_0 = 2, J_2 = 2\}$ and $\{J_0 = 0.2, J_2 = 0.5\}$, respectively. The transition points agree with the closing points of the bulk gap. Figures 6(c) and 6(d) show the phase diagrams of ν in the J_0 - g plane with $J_2 = 0.5$ and 1.5 , respectively. By increasing g , the system can experience the topological transitions $\nu = 2 \rightarrow \nu = 1$ and $0 \rightarrow \nu = 1$.

Remarkably, the topology of one-dimensional non-Hermitian chiral-symmetric systems [i.e., $\eta H^\dagger(k)\eta^{-1} = -H(k)$] can also be characterized by a hidden Chern number [62]. This Chern number is described by an effective two-dimensional Hermitian Hamiltonian $H_{\text{eff}}(k, \epsilon) = \eta[\epsilon - iH(k)]$, where ϵ is the imaginary part of the energy. From Eq. (4), the effective Hamiltonian of our

system is

$$H_{\text{eff}}(k, \epsilon) = \begin{pmatrix} \epsilon + g & -ih_k & 0 & -iJ_2 e^{-ik} \\ ih_k^* & g - \epsilon & iJ_2 & 0 \\ 0 & -iJ_2 & \epsilon - g & -ih_k \\ iJ_2 e^{ik} & 0 & ih_k^* & -\epsilon - g \end{pmatrix}. \quad (8)$$

In order to overcome the periodicity of ϵ , we take $H'_{\text{eff}}(k, \epsilon) = R_\epsilon H_{\text{eff}}(k, \epsilon) R_\epsilon^\dagger$ with $R_\epsilon = \exp[i\frac{\pi}{4}(1 + \tanh \epsilon)G]$ and $G = \sigma_x \otimes \sigma_0$. In this case, $H'_{\text{eff}}(k, \epsilon \rightarrow -\infty) = H'_{\text{eff}}(k, \epsilon \rightarrow +\infty) = -|\epsilon|\eta$. It should be noticed that the energy spectrum of H'_{eff} is consistent with H_{eff} . The Chern number \mathcal{C} of the Hamiltonian (8) can be obtained as [63]

$$\mathcal{C} = \frac{1}{2\pi} \int_{-\infty}^{+\infty} d\epsilon \int_{-\pi}^{\pi} dk \Omega_{k,\epsilon}, \quad (9)$$

where the Berry curvature

$$\Omega_{k,\epsilon} = \sum_{\substack{n \leq n_F \\ m > n_F}} \text{Im} \frac{2 \langle \phi_{k,\epsilon}^n | \partial_k H'_{\text{eff}} | \phi_{k,\epsilon}^m \rangle \langle \phi_{k,\epsilon}^m | \partial_\epsilon H'_{\text{eff}} | \phi_{k,\epsilon}^n \rangle}{(E_{k,\epsilon}^n - E_{k,\epsilon}^m)^2}. \quad (10)$$

Here, $|\phi_{k,\epsilon}^n\rangle$ is the eigenstate of $H_{\text{eff}}(k, \epsilon)$ with eigenvalue $E_{k,\epsilon}^n$, and n_F is the number of occupied bands.

In Figs. 7(a)–7(c) and 7(d)–7(f), we plot the band structures of the effective Hermitian Hamiltonian (8) for different g with $\{J_0 = 2, J_2 = 2\}$ and $\{J_0 = 0.2, J_2 = 0.5\}$, respectively. It is clear that the middle pair of bands closes at critical points $g = \sqrt{5}$ and $\sqrt{1.19}$, respectively. This suggests the occurrence of topological phase transition described by the Chern number defined in the ϵ - k space. The calculated Chern number is shown in Figs. 7(g) and 7(h). We find that the non-Hermiticity can drive the topological transition from $\mathcal{C} = -2$ to -1 and $\mathcal{C} = 0$ to -1 . The transition points agree with the non-Hermitian winding number shown in Figs. 6(a) and 6(b). According to bulk-boundary correspondence, the zero-energy edge states can also be obtained from the Hamiltonian $H_{\text{obc}}^{\text{eff}}(k, \epsilon) = \eta[\epsilon - iH_{\text{obc}}]$, where H_{obc} is the Hamiltonian (1) with the open boundary condition. In Figs. 7(i) and 7(j), we show the phase diagrams of \mathcal{C} in the J_0 - g plane for $J_2 = 0.5$ and 1.5 , respectively. It can be seen that the phase boundaries are consistent with those in Figs. 6(c) and 6(d).

IV. NON-HERMITICITY-INDUCED TOPOLOGICAL PHASE TRANSITIONS IN THE MORE GENERAL LONG-RANGE SSH MODEL

In Secs. II and III, we focus on the non-Hermitian SSH mode with the third nearest-neighbor hoppings. The maximum winding number is $\nu = 2$. In this section, we extend the above discussions to a more general long-range SSH model with the higher winding number and further demonstrate the influences of the non-Hermiticity.

As shown in Fig. 8(a), we consider the long-range SSH model with both the third and fourth nearest-neighbor hoppings J_0 and J'_0 . The gain and loss are introduced as the same in Fig. 1(a). Note that both long-range hoppings preserve the chiral symmetry of the system. The Hamiltonian of the Hermitian long-range SSH lattice is $H'_x(k) = h'_x \sigma_x + h'_y \sigma_y$ with $h'_x = J_1 + J_2 \cos k + J_0 \cos(2k) + J'_0 \cos(3k)$ and

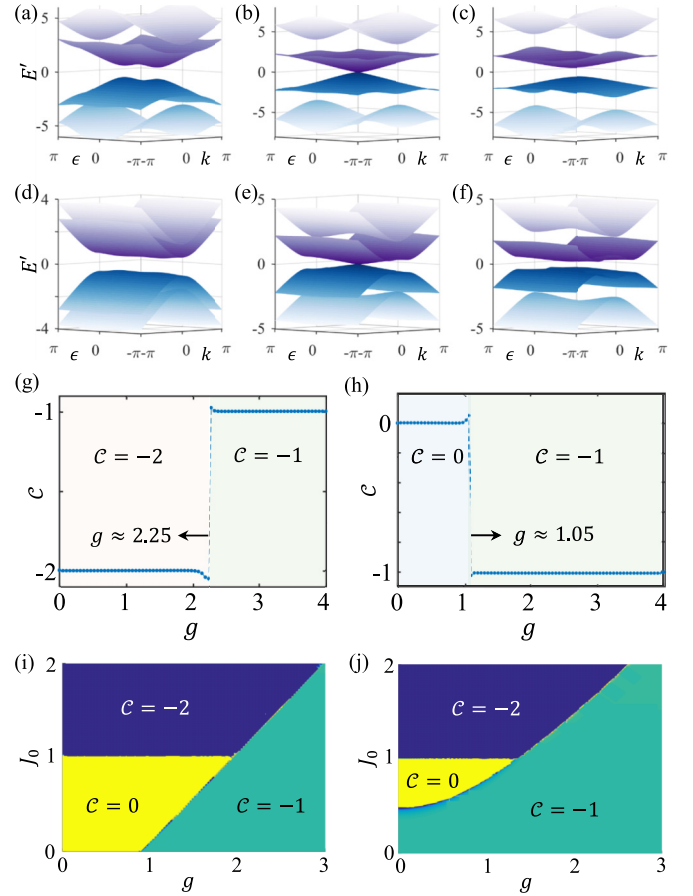


FIG. 7. (a–c) Band structures of the Hamiltonian (8) for $g = 1$ (a), $g = \sqrt{5}$ (b), and $g = 3$ (c), when $J_0 = 2$ and $J_2 = 2$. (d–f) Band structures of the Hamiltonian (8) for $g = 0.5$ (d), $g = \sqrt{1.19}$ (e), and $g = 1.5$ (f), when $J_0 = 0.2$ and $J_2 = 0.5$. (g, h) The corresponding Chern number \mathcal{C} as a function of g , when $\{J_0 = 2, J_2 = 2\}$ (g) and $\{J_0 = 0.2, J_2 = 0.5\}$ (h). (i, j) Phase diagrams of \mathcal{C} in the J_0 - g plane for $J_2 = 0.5$ and $J_2 = 1.5$, respectively.

$h'_y = J_1 + J_2 \sin k + J_0 \sin(2k) + J'_0 \sin(3k)$. Considering the non-Hermitian gain and loss, the Hamiltonian in the momentum space is obtained as

$$H'(k) = \begin{pmatrix} ig & h_k & 0 & h'_k \\ h_k^* & -ig & J_2 + J'_0 e^{ik} & 0 \\ 0 & J_2 + J'_0 e^{-ik} & -ig & h_k \\ h_k^* & 0 & h_k^* & ig \end{pmatrix}, \quad (11)$$

where $h'_k = J_2 e^{-ik} + J'_0 e^{-2ik}$.

When $J_0 = 0$ and $J'_0 \neq 0$, the system has three topological phases characterized by $w = \{0, 1, 3\}$ without non-Hermiticity, as shown in Fig. 8(b). The non-Hermitian parameter only drives a topological phase transition from a trivial phase to a nontrivial phase with $\nu = 1$ [Fig. 8(c)]. However, when both J_0 and J'_0 exist, the Hermitian system has richer topological phases with $w = \{0, 1, 2, 3\}$ [Fig. 8(d)]. In this case, the non-Hermiticity drives the system from $\nu = 0$ to 1 and from $\nu = 2$ to 3, as shown in Fig. 8(e). These results indicate that the topological transitions driven by the

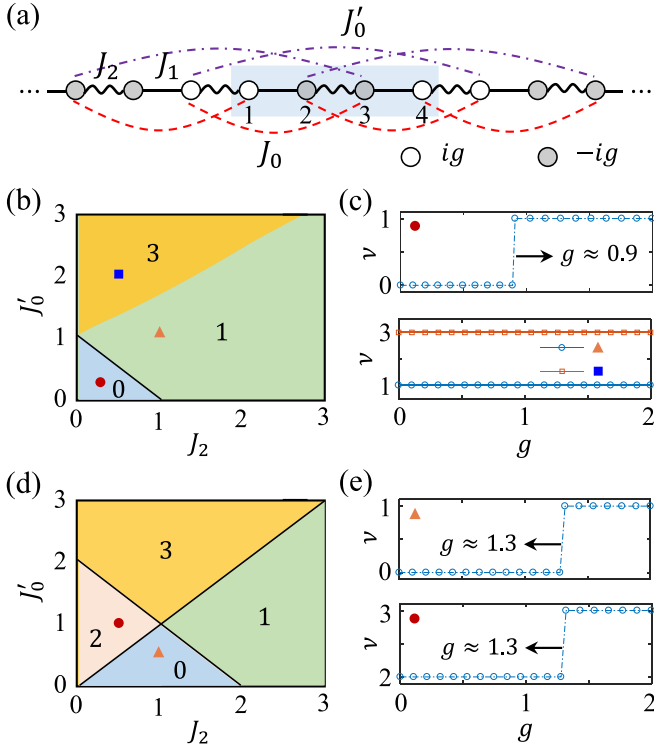


FIG. 8. (a) Schematic of the non-Hermitian SSH model with long-range hoppings J_0 (red dashed lines) and J'_0 (dash-dotted lines). (b) Phase diagram of the Hermitian long-range SSH model for the winding number $w = \{0, 1, 3\}$, when $J_0 = 0$ and $J'_0 \neq 0$. (c) Non-Hermitian winding number ν as functions of g , when $\{J_2 = 0.2, J'_0 = 0.2\}$ (upper panel) and $\{J_2 = 1, J'_0 = 1\}$ and $\{J_2 = 0.5, J'_0 = 2\}$ (lower panel). (d) Phase diagram of the Hermitian long-range SSH model for the winding number $w = \{0, 1, 2, 3\}$, when $J_0 \neq 0$ and $J'_0 \neq 0$. We set $J_0 = J_1 = 1$. (e) Non-Hermitian winding number ν as functions of g , when $\{J_2 = 1, J'_0 = 0.5\}$ (upper panel) and $\{J_2 = 0.5, J'_0 = 1\}$ (lower panel).

non-Hermiticity are closely related to the topological phase of the corresponding Hermitian case.

In Table I, we summarize the main results of the non-Hermiticity-induced topological phase transitions in the general long-range SSH model. We conclude that the non-Hermiticity can induce topological transitions from ν_ρ to $\nu_{\rho \pm 1}$ with the following constraints.

TABLE I. Summary of results for the non-Hermiticity-induced TPTs in a long-range SSH model. J_1 and J_2 denote the intra- and intercell hopping strengths, and J_0 and J'_0 denote the third and the fourth nearest-neighbor long-range hoppings. w is the winding number without non-Hermiticity and ν is the winding number in the presence of non-Hermiticity.

Hopping amplitudes	Hermitian topological phases	Non-Hermiticity-induced TPTs
J_1, J_2	$w = \{0, 1\}$	$\nu = 0 \rightarrow \nu = 1$
J_1, J_2, J_0	$w = \{0, 1, 2\}$	$\nu = 0 \rightarrow \nu = 1, \nu = 2 \rightarrow \nu = 1$
J_1, J_2, J'_0	$w = \{0, 1, 3\}$	$\nu = 0 \rightarrow \nu = 1$
J_1, J_2, J_0, J'_0	$w = \{0, 1, 2, 3\}$	$\nu = 0 \rightarrow \nu = 1, \nu = 2 \rightarrow \nu = 3$

- (i) The winding number $\nu_\rho = \rho$ is an even number.
- (ii) The topological phases with $\{\nu_\rho, \nu_{\rho \pm 1}\}$ also exist in the corresponding Hermitian case.
- (iii) If the maximum winding number of the system is equal to ν_ρ , the non-Hermiticity drives the topological transitions $\nu_\rho \rightarrow \nu_{\rho-1}$; otherwise, the non-Hermiticity drives the topological transitions $\nu_\rho \rightarrow \nu_{\rho+1}$.

V. PROPOSAL FOR CIRCUIT DEMONSTRATION

Recently, electric circuits have been regarded as a powerful platform for synthetic topological matter [64,65]. Because of the wide choice of circuit components, electric circuits provide us with unprecedented convenience and flexibility in engineering non-Hermitian topological insulators with non-reciprocal hoppings or on-site gain and loss [55,66,67]. In this section, we propose a possible experimental scheme by employing electrical circuits to simulate the non-Hermiticity-induced topological phase transition.

As shown in Fig. 9, the staggered nearest-neighbor hoppings are represented by capacitors C_1 and C_2 , and the long-range hopping is represented by capacitors C_0 . The on-site gain and loss are introduced by the resistive elements R and R' . According to Kirchhoff's law, the response of the circuit at frequency ω is given by $\mathbf{I}(\omega) = \mathbf{J}(\omega)\mathbf{V}(\omega)$, where \mathbf{I} denotes the current input and \mathbf{V} is the voltage measured against ground at each node, and \mathbf{J} is the circuit Laplacian. The Hamiltonian (1) can be implemented through $\mathbf{J}(\omega)$. Considering the periodic boundary condition, the bulk-circuit Laplacian in the momentum space (Fig. 9) is written as

$$\mathbf{J}(\omega, k) = i\omega \begin{pmatrix} \sigma_1 & J_{12} & 0 & -C_2 e^{-ik} \\ J_{12}^* & \sigma_2 & -C_2 & 0 \\ 0 & -C_2 & \sigma_3 & J_{34} \\ -C_2 e^{ik} & 0 & J_{34}^* & \sigma_4 \end{pmatrix}, \quad (12)$$

where $\sigma_{1,4} = C_0 + C_1 + C_2 - \frac{1}{\omega^2 L_0} + \frac{1}{i\omega R}$, $\sigma_{2,3} = C_0 + C_1 + C_2 - \frac{1}{\omega^2 L_0} + \frac{1}{i\omega R'}$, and $J_{12} = J_{34} = -(C_1 + C_0 e^{-ik})$. By setting the midgap frequency $\omega_0 = [(C_0 + C_1 + C_2)L_0]^{-1/2}$, the inductive and capacitive components in the diagonal terms are canceled out. The non-Hermitian gain and loss terms are realized by employing the negative and positive resistors. The negative impedance converter can be used to implement gain (negative resistance).

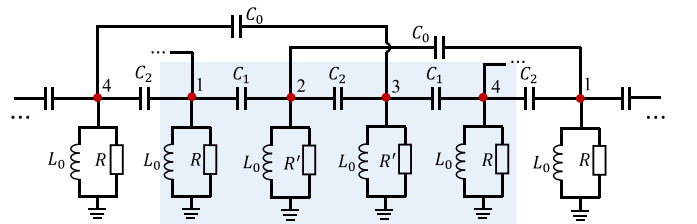


FIG. 9. The scheme of the electric circuit to simulate the Hamiltonian (1). $C_{0,1,2}$ denote the capacitances of the capacitors, which simulate the hoppings. The on-site gain and loss are controlled by the resistive elements R and R' . The inductor L_0 tunes the resonance frequency of the circuit.

The response of the system to a given input current signal is governed by the eigenstates of $\mathbf{J}(\omega)$. In the experiment, we can measure the admittance band structure with periodic boundary condition and the eigenstates (eigenvalues) with open boundary condition. By tuning the positive and negative resistors in the circuit, the system can switch between different topological phase regions. In addition to the electric circuits, a photonic resonator network with synthetic dimensions [68] is also a promising platform to simulate the non-Hermiticity-induced topological transitions of this paper.

VI. CONCLUSIONS

In summary, we have studied topological transitions in a non-Hermitian long-range SSH model, in which the complex on-site potential ($ig, -ig, -ig, ig$) and the third nearest-neighbor hopping are included. By analyzing the bulk band gap, topological edge states, and complex Zak phase, we

found that the non-Hermiticity can drive topological transitions $\nu = 0 \rightarrow 1$ and $2 \rightarrow 1$. We have also investigated the impacts of non-Hermiticity on the topological properties in a more general long-range SSH model. It is found that the non-Hermiticity can drive exotic topological transitions associated with the topological phases of the corresponding Hermitian case. Finally, we have proposed a feasible experimental scheme to realize such non-Hermiticity-induced topological transitions. Our paper may pave the way for the study of non-Hermitian topological states and their device applications.

ACKNOWLEDGMENTS

This work is supported partly by the National Key R&D Program of China under Grant No. 2021YFA1400900 and the National Natural Science Foundation of China under Grants No. 12034012, No. 12074232, No. 12125406, and No. 1331KSC.

-
- [1] V. V. Konotop, J. Yang, and D. A. Zezyulin, Nonlinear waves in PT-symmetric systems, *Rev. Mod. Phys.* **88**, 035002 (2016).
 - [2] R. El-Ganainy, K. G. Makris, M. Khajavikhan, Z. H. Musslimani, S. Rotter, and D. N. Christodoulides, Non-Hermitian physics and PT symmetry, *Nat. Phys.* **14**, 11 (2018).
 - [3] C. M. Bender, Making sense of non-Hermitian Hamiltonians, *Rep. Prog. Phys.* **70**, 947 (2007).
 - [4] Y. Ashida, Z. Gong, and M. Ueda, Non-Hermitian physics, *Adv. Phys.* **69**, 249 (2020).
 - [5] S. K. Özdemir, S. Rotter, F. Nori, and L. Yang, Parity-time symmetry and exceptional points in photonics, *Nat. Mater.* **18**, 783 (2019).
 - [6] C. E. Rüter, K. G. Makris, R. El-Ganainy, D. N. Christodoulides, M. Segev, and D. Kip, Observation of parity-time symmetry in optics, *Nat. Phys.* **6**, 192 (2010).
 - [7] D. C. Brody, Biorthogonal quantum mechanics, *J. Phys. A* **47**, 035305 (2014).
 - [8] W. D. Heiss, The physics of exceptional points, *J. Phys. A* **45**, 444016 (2012).
 - [9] M.-A. Miri and A. Alù, Exceptional points in optics and photonics, *Science* **363**, eaar7709 (2019).
 - [10] S. Weidemann, M. Kremer, S. Longhi, and A. Szameit, Coexistence of dynamical delocalization and spectral localization through stochastic dissipation, *Nat. Photonics* **15**, 576 (2021).
 - [11] C. Wu, J. Fan, G. Chen, and S. Jia, Non-Hermiticity-induced reentrant localization in a quasiperiodic lattice, *New J. Phys.* **23**, 123048 (2021).
 - [12] E. J. Bergholtz, J. C. Budich, and F. K. Kunst, Exceptional topology of non-Hermitian systems, *Rev. Mod. Phys.* **93**, 015005 (2021).
 - [13] H. Wang, X. Zhang, J. Hua, D. Lei, M. Lu, and Y. Chen, Topological physics of non-Hermitian optics and photonics: A review, *J. Opt.* **23**, 123001 (2021).
 - [14] T. E. Lee, Anomalous Edge State in a Non-Hermitian Lattice, *Phys. Rev. Lett.* **116**, 133903 (2016).
 - [15] A. Ghatak and T. Das, New topological invariants in non-hermitian systems, *J. Phys.: Condens. Matter* **31**, 263001 (2019).
 - [16] H. Jiang, C. Yang, and S. Chen, Topological invariants and phase diagrams for one-dimensional two-band non-Hermitian systems without chiral symmetry, *Phys. Rev. A* **98**, 052116 (2018).
 - [17] D. Leykam, K. Y. Bliokh, C. Huang, Y. D. Chong, and F. Nori, Edge Modes, Degeneracies, and Topological Numbers in Non-Hermitian Systems, *Phys. Rev. Lett.* **118**, 040401 (2017).
 - [18] S. Yao and Z. Wang, Edge States and Topological Invariants of Non-Hermitian Systems, *Phys. Rev. Lett.* **121**, 086803 (2018).
 - [19] F. Song, S. Yao, and Z. Wang, Non-Hermitian Skin Effect and Chiral Damping in Open Quantum Systems, *Phys. Rev. Lett.* **123**, 170401 (2019).
 - [20] S. Longhi, Probing non-Hermitian skin effect and non-Bloch phase transitions, *Phys. Rev. Research* **1**, 023013 (2019).
 - [21] K. Zhang, Z. Yang, and C. Fang, Correspondence between Winding Numbers and Skin Modes in Non-Hermitian Systems, *Phys. Rev. Lett.* **125**, 126402 (2020).
 - [22] C.-H. Liu, K. Zhang, Z. Yang, and S. Chen, Helical damping and dynamical critical skin effect in open quantum systems, *Phys. Rev. Research* **2**, 043167 (2020).
 - [23] Z. Gong, Y. Ashida, K. Kawabata, K. Takasan, S. Higashikawa, and M. Ueda, Topological Phases of Non-Hermitian Systems, *Phys. Rev. X* **8**, 031079 (2018).
 - [24] L. Li, C. H. Lee, S. Mu, and J. Gong, Critical non-Hermitian skin effect, *Nat. Commun.* **11**, 5491 (2020).
 - [25] R. Okugawa, R. Takahashi, and K. Yokomizo, Second-order topological non-Hermitian skin effects, *Phys. Rev. B* **102**, 241202(R) (2020).
 - [26] K. Yokomizo and S. Murakami, Non-Bloch Band Theory of Non-Hermitian Systems, *Phys. Rev. Lett.* **123**, 066404 (2019).
 - [27] Z. Yang, K. Zhang, C. Fang, and J. Hu, Non-Hermitian Bulk-Boundary Correspondence and Auxiliary Generalized Brillouin Zone Theory, *Phys. Rev. Lett.* **125**, 226402 (2020).
 - [28] H. Shen, B. Zhen, and L. Fu, Topological Band Theory for Non-Hermitian Hamiltonians, *Phys. Rev. Lett.* **120**, 146402 (2018).
 - [29] S. Yao, F. Song, and Z. Wang, Non-Hermitian Chern Bands, *Phys. Rev. Lett.* **121**, 136802 (2018).

- [30] F. K. Kunst, E. Edvardsson, J. C. Budich, and E. J. Bergholtz, Biorthogonal Bulk-Boundary Correspondence in Non-Hermitian Systems, *Phys. Rev. Lett.* **121**, 026808 (2018).
- [31] L. Jin and Z. Song, Bulk-boundary correspondence in a non-Hermitian system in one dimension with chiral inversion symmetry, *Phys. Rev. B* **99**, 081103(R) (2019).
- [32] S. Longhi, Non-Bloch-Band Collapse and Chiral Zener Tunneling, *Phys. Rev. Lett.* **124**, 066602 (2020).
- [33] L. Xiao, T. Deng, K. Wang, G. Zhu, Z. Wang, W. Yi, and P. Xue, Non-Hermitian bulk-boundary correspondence in quantum dynamics, *Nat. Phys.* **16**, 761 (2020).
- [34] Y. Xu, S.-T. Wang, and L.-M. Duan, Weyl Exceptional Rings in a Three-Dimensional Dissipative Cold Atomic Gas, *Phys. Rev. Lett.* **118**, 045701 (2017).
- [35] A. Cerjan, S. Huang, M. Wang, K. P. Chen, Y. Chong, and M. C. Rechtsman, Experimental realization of a Weyl exceptional ring, *Nat. Photonics* **13**, 623 (2019).
- [36] K. Kawabata, K. Shiozaki, M. Ueda, and M. Sato, *Phys. Rev. X* **9**, 041015 (2019).
- [37] K. Kawabata, S. Higashikawa, Z. Gong, Y. Ashida, and M. Ueda, Topological unification of time-reversal and particle-hole symmetries in non-Hermitian physics, *Nat. Commun.* **10**, 297 (2019).
- [38] C.-H. Liu, H. Jiang, and S. Chen, Topological classification of non-Hermitian systems with reflection symmetry, *Phys. Rev. B* **99**, 125103 (2019).
- [39] H. Zhou and J. Y. Lee, Periodic table for topological bands with non-Hermitian symmetries, *Phys. Rev. B* **99**, 235112 (2019).
- [40] B. Bahari, A. Ndao, F. Vallini, A. E. Amili, Y. Fainman, and B. Kanté, Nonreciprocal lasing in topological cavities of arbitrary geometries, *Science* **358**, 636 (2017).
- [41] M. Parto, S. Wittek, H. Hodaei, G. Harari, M. A. Bandres, J. Ren, M. C. Rechtsman, M. Segev, D. N. Christodoulides, and M. Khajavikhan, Edge-Mode Lasing in 1D Topological Active Arrays, *Phys. Rev. Lett.* **120**, 113901 (2018).
- [42] J. C. Budich and E. J. Bergholtz, Non-Hermitian Topological Sensors, *Phys. Rev. Lett.* **125**, 180403 (2020).
- [43] A. McDonald and A. A. Clerk, Exponentially-enhanced quantum sensing with non-Hermitian lattice dynamics, *Nat. Commun.* **11**, 5382 (2020).
- [44] F. Koch and J. C. Budich, Quantum non-Hermitian topological sensors, *Phys. Rev. Research* **4**, 013113 (2022).
- [45] S. Weidemann, M. Kremer, T. Helbig, T. Hofmann, A. Stegmaier, M. Greiter, R. Thomale, and A. Szameit, Topological funneling of light, *Science* **368**, 311 (2020).
- [46] H. Zhao, X. Qiao, T. Wu, B. Midya, S. Longhi, and L. Feng, Non-Hermitian topological light steering, *Science* **365**, 1163 (2019).
- [47] J. M. Zeuner, M. C. Rechtsman, Y. Plotnik, Y. Lumer, S. Nolte, M. S. Rudner, M. Segev, and A. Szameit, Observation of a Topological Transition in the Bulk of a Non-Hermitian System, *Phys. Rev. Lett.* **115**, 040402 (2015).
- [48] S. Lieu, Topological phases in the non-Hermitian Su-Schrieffer-Heeger model, *Phys. Rev. B* **97**, 045106 (2018).
- [49] L. Du, J.-H. Wu, M. Artoni, and G. C. L. Rocca, Phase-dependent topological interface state and spatial adiabatic passage in a generalized Su-Schrieffer-Heeger model, *Phys. Rev. A* **100**, 012112 (2019).
- [50] F. Dangel, M. Wagner, H. Cartarius, J. Main, and G. Wunner, Topological invariants in dissipative extensions of the Su-Schrieffer-Heeger model, *Phys. Rev. A* **98**, 013628 (2018).
- [51] K. Takata and M. Notomi, Photonic Topological Insulating Phase Induced Solely by Gain and Loss, *Phys. Rev. Lett.* **121**, 213902 (2018).
- [52] H. C. Wu, L. Jin, and Z. Song, Topology of an anti-parity-time symmetric non-Hermitian Su-Schrieffer-Heeger model, *Phys. Rev. B* **103**, 235110 (2021).
- [53] J.-R. Li, L.-L. Zhang, W.-B. Cui, and W.-J. Gong, Topological properties in non-Hermitian tetratomic Su-Schrieffer-Heeger lattices, *Phys. Rev. Research* **4**, 023009 (2022).
- [54] H. Gao, H. Xue, Q. Wang, Z. Gu, T. Liu, J. Zhu, and B. Zhang, Observation of topological edge states induced solely by non-Hermiticity in an acoustic crystal, *Phys. Rev. B* **101**, 180303(R) (2020).
- [55] S. Liu, S. Ma, C. Yang, L. Zhang, W. Gao, Y. J. Xiang, T. J. Cui, and S. Zhang, Gain- and Loss-Induced Topological Insulating Phase in a Non-Hermitian Electrical Circuit, *Phys. Rev. Applied* **13**, 014047 (2020).
- [56] H. Xue, Q. Wang, B. Zhang, and Y. D. Chong, Non-Hermitian Dirac Cones, *Phys. Rev. Lett.* **124**, 236403 (2020).
- [57] H. T. Teo, H. Xue, and B. Zhang, Topological phase transition induced by gain and loss in a photonic Chern insulator, *Phys. Rev. A* **105**, 053510 (2022).
- [58] X.-W. Luo and C. Zhang, Higher-Order Topological Corner States Induced by Gain and Loss, *Phys. Rev. Lett.* **123**, 073601 (2019).
- [59] Y.-J. Wu, C.-C. Liu, and J. Hou, Wannier-type photonic higher-order topological corner states induced solely by gain and loss, *Phys. Rev. A* **101**, 043833 (2020).
- [60] J. Hou, Y.-J. Wu, and C. Zhang, Topological phase transitions driven by non-Hermiticity in quantum spin Hall insulators, *Phys. Rev. B* **103**, 205110 (2021).
- [61] S.-D. Liang and G.-Y. Huang, Topological invariance and global Berry phase in non-Hermitian systems, *Phys. Rev. A* **87**, 012118 (2013).
- [62] W. Brzezicki and T. Hyart, Hidden Chern number in one-dimensional non-Hermitian chiral-symmetric systems, *Phys. Rev. B* **100**, 161105(R) (2019).
- [63] M. Z. Hasan and C. L. Kane, Colloquium: Topological insulators, *Rev. Mod. Phys.* **82**, 3045 (2010).
- [64] V. Albert, L. I. Glazman, and L. Jiang, Topological Properties of Linear Circuit Lattices, *Phys. Rev. Lett.* **114**, 173902 (2015).
- [65] C. H. Lee, S. Imhof, C. Berger, F. Bayer, J. Brehm, L. W. Molenkamp, T. Kiessling, and R. Thomale, Topoelectrical circuits, *Commun. Phys.* **1**, 39 (2018).
- [66] T. Helbig, T. Hofmann, S. Imhof, M. Abdelghany, T. Kiessling, L. W. Molenkamp, C. H. Lee, A. Szameit, M. Greiter, and R. Thomale, Generalized bulk-boundary correspondence in non-Hermitian topoelectrical circuits, *Nat. Phys.* **16**, 747 (2020).
- [67] A. Stegmaier, S. Imhof, T. Helbig, T. Hofmann, C. H. Lee, M. Kremer, A. Fritzsche, T. Feichtner, S. Klemmt, S. Höfling, I. Boettcher, I. C. Fulga, O. G. Schmidt, M. Greiter, T. Kiessling, A. Szameit, and R. Thomale, Topological Defect Engineering and PT-Symmetry in Non-Hermitian Electrical Circuits, *Phys. Rev. Lett.* **126**, 215302 (2021).
- [68] C. Leefmans, A. Dutt, J. Williams, L. Yuan, M. Parto, F. Nori, S. Fan, and A. Marandi, Topological dissipation in a time-multiplexed photonic resonator network, *Nat. Phys.* **18**, 442 (2022).